Evaluation of Phosphate Tridecyl Ethoxylate Triethanolamine Salt as a Corrosion Inhibitor in CO_2-O_2 Environment for Carbon Steel

Roberta B. Vasques[a] (ORCID), *Carlos Vinicius R.P. de Queiroz[a], Marjory M. Levy[a],*

Paulo Vitor M. da Silva[a], Gustavo L. Vaz[b], Eliane D'Elia[c] (ORCID)*, Álvaro A.O. Magalhães[b],*

Walney S. Araújo[a]* (ORCID)

[a] Universidade Federal do Ceará, Departamento de Engenharia Metalúrgica, 60440-900, Fortaleza, CE, Brasil.
[b] Centro de Pesquisa da Petrobras, 21941-915, Ilha do Fundão, Rio de Janeiro, RJ, Brasil.
[c] Universidade Federal do Rio de Janeiro, Instituto de Química, 21941-909, Rio de Janeiro, RJ, Brasil.

Investigation of corrosion inhibitors on CO_2-saturated aqueous solution with O_2 contamination is limited. Hence, this study investigated the corrosion behavior of phosphate ester inhibitor towards carbon steel corrosion in a simulated CO_2-O_2 environment by potentiodynamic polarization technique and electrochemical impedance spectroscopy. It was shown that the PE prevents the corrosion attack in the presence of CO_2-O_2, reaching an efficiency of 90.7% with 25 ppm in 3.5 *wt*% NaCl solution at 25 °C. Furthermore, the superficial characterization of carbon steel was studied by scanning electronic microscopy which supported that the inhibitor protects against corrosion. The varying temperatures showed that PE adsorbed on the steel surface by a physical process and obeyed the Langmuir isotherm.

Keywords: *Inhibitor, phosphate ester, CO_2 corrosion, O_2 corrosion.*

1. Introduction

Corrosion is a major problem that generates costs and losses for industries. In oil and gas processing, the challenges related to combating corrosion are enormous due to the presence of several dissolved ions and gases (CO_2, O_2, H_2S) with high corrosive potential throughout the exploration and transportation stages[1-3]. To mitigate the corrosion effects, the addition of organic substances as corrosion inhibitors is the most common and practical method[4].

The study of the CO_2 corrosion mechanism has been widely discussed in the literature, as well as the utilization of corrosion inhibitors for CO_2-saturated under different operating conditions (pH, temperature, and pressure)[5-13]. However, another concern of the oil industry is the influence of small concentrations of dissolved O_2 (DO) on the corrosion of carbon steel and the anticorrosive performance of inhibitors in the presence of CO_2 saturation.

Firstly, the small amounts of DO in oilfield systems accelerate the corrosion rate by an additional cathodic reaction. Secondly, O_2 could hinder the deposition of protective iron carbonate ($FeCO_3$) by oxidizing ferrous ions to ferric ions, resulting in a non-protective iron oxide film production, and finally, may reduce the efficacy of corrosion inhibition[14-16]. Hence, the application of organic substances in a CO_2-O_2 medium is scarce, and the action of typical CO_2 corrosion inhibitors does not present a similar performance of inhibition efficiency in the presence of oxygen[17,18].

Phosphate esters (PE) are active surface anionic components applied as corrosion inhibitors due to their effective behavior at moderate temperatures and/or in small amounts of dissolved oxygen. Yepez et al.[19] reported that a novel phosphate ester was superior to imidazoline in the presence of oxygen and CO_2 through the strong interaction with oxidized surfaces. Moreover, the suggested mechanism was by deactivation coverage mechanism[20].

Alkyl phosphate ester derivate was another molecule that was also shown to be a potential inhibitor for CO_2-O_2 environments. Bis(2-ethyl hexyl) phosphate (BEP) was investigated in 1 *wt*.% NaCl solution at 50 °C, controlling the O_2 concentration. The results showed that the high O_2 concentration enhances the cathodic reaction and hinders the formation of an inhibitor layer on the steel surface. Hence, the low O_2 concentration obtained a better inhibition efficiency. Furthermore, the authors studied through molecular dynamics that the BEP anions adsorb more easily on the carbon steel surface than O_2 and H_2O[21].

As mentioned above, complications arise in the CO_2 corrosion process of steel due to the presence of oxygen. Research into corrosion inhibitors in CO_2-saturated solutions contaminated with O_2 is restricted, and the mechanism that diminishes inhibitor performance in the presence of small amounts of oxygen has not been fully comprehended. The phosphate esters and their derivatives appear promising candidates for CO_2-O_2 corrosion inhibition, provided they also demonstrate advantages in competing for adsorption with O_2. Therefore, the main purpose of this paper is to

investigate the corrosion minimization of AISI 1018 steel in a CO2-saturated NaCl solution with O_2 contamination by using a tridecyl ethoxylate triethanolamine salt. Various experimental techniques were employed to demonstrate the relative inhibition performance. Moreover, we report on the effects of evaluating operating conditions on selecting the optimum corrosion inhibitor dosage. Surface analysis was carried out to characterize and inspect the reliability of the inhibition phenomenon.

2. Materials and Methods

2.1. Materials and solution

The AISI 1018 low carbon steel samples were of the following compositions (*wt.*%): C 0.197, Mn 0.84, Si 0.19, Fe balance. The AISI 1018 samples for electrochemical testing were soldered on the surface with insulated copper wire and coated with epoxy resin. The preparation process before each test consisted of wet grinding each specimen successively with 220, 320, 400, and 600 silicon carbide (SiC) grit papers. Samples were then rinsed with distilled water and ethanol before being dried using compressed air.

The inhibitor molecule used in this study was Phosphate tridecyl ethoxylate triethanolamine salt, whose molecular structure is shown in Figure 1. Spectroscopic analysis of the inhibitor molecule was carried out using a Fourier transform infrared spectrophotometer (Spectrum Frontier, Perkin-Elmer Corp., Norwalk, USA) equipped with a crystal to perform attenuated total reflectance (ATR-FTIR) analysis. The spectra were obtained in a 4000–600 cm–1 spectral range with a 2 *cm^{-1}* resolution in transmittance mode. Figure 1 illustrates the FTIR spectra with the characteristic bonds identified.

2.2. Electrochemical measurements

Autolab Potentiostat with Autolab NOVA 2.1 software was used in all the electrochemical measurements. The conventional
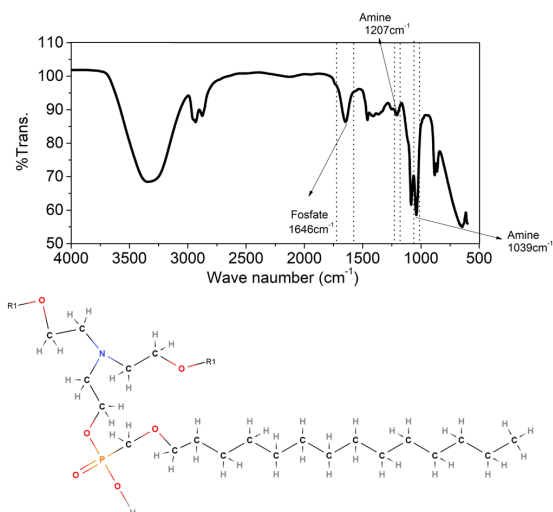
three-electrode cell was used, with a platinum grid as a counter electrode and Hastelloy as a pseudo-reference electrode. The traditional reference electrode (Ag/AgCl or saturated calomel) used in electrochemical tests cannot be applied in this system because the inhibitor penetrates through the porous tip and contaminates the internal solution[22]. Before each experiment, the NaCl solution was purged with N_2 (high purity> 99.998%) for 15 minutes. Then, a mixed gas (CO_2-O_2) was bubbled until it reached 500 ppm of O_2 concentration through VisiFerm Dissolved Oxygen Sensors from Hamilton®. Afterward, the sample was immersed for 1 h before the electrochemical measurements. The experiments were performed in 3.5 *wt.*% NaCl solution with different PE concentrations from 25 to 60 °C, at pH 4.

Electrochemical impedance spectroscopy (EIS) was taken at the open circuit potential (OCP) with a frequency range from 10 kHz to 6 mHz and a disturbance of 10 mV rms. The polarization curves were obtained in the range –200 to +200 mV versus E_{ocp} at a scan rate of 10 mV s^{-1}). Each test was repeated three times to verify its reproducibility. The inhibition efficiency (η%) was calculated utilizing the charge transfer resistance from EIS diagrams, R_{ct}, with and without inhibitor, as shown in Equation 1[23]:

$$\eta\% = (R_{ct(Inh)} - R_{ct(Blank)}) / R_{ct(inh)} x100 \qquad (1)$$

2.3. Weight loss measurements

Weight loss tests were performed according to ASTM G1[24] procedures in 3.5 *wt.*% NaCl solution with continuous bubbling mixed CO_2-O_2 gas (low dissolved oxygen, 500 ppb) and an immersion time of 8 h. The higher concentration of the inhibitor presented the best performance in the electrochemical test, 25 ppm was chosen to be tested in different temperatures, 25, 40, and 60 °C. Cylindrical carbon steel 1018 with 8 cm² was used. Each experiment was carried out in triplicate. The *CR* (corrosion rate, in mm/y) was calculated using Equation 2[25]:

$$CR = 87.6.W / d.A.t \qquad (2)$$

Where A is the specimen surface area in cm², W is the weight loss in mg, t is the immersion time in hours, and d is the specimen density in g cm^{-3}. The inhibition efficiency (*IE%*) was calculated using Equation 3[25]:

$$\eta\% = (CR_{Blank} - CR_{Inh}) / CR_{Blank} x100 \qquad (3)$$

where CR_{blank} is the corrosion rate (mmy) in the absence of the inhibitor and CR_{inh} is the corrosion rate (mmy) in the presence of the inhibitor.

The apparent activation energy (E_a) of C1018 corrosion in medium containing CO_2/O_2, the kinetic parameter related to CR_{inh} was calculated according to Arrhenius equation[25]:

$$\log CR = -(E_a / 2.303R.T) + \ln A \qquad (4)$$

where R is the gas constant, and T is the absolute temperature.

Figure 1. The general structure and FTIR spectra obtained of Ethanol, 2,2,2-nitrilotris compound with alphatridecylomega- hydroxypoly (oxy-1,2-ethanediyl) phosphate molecule (PE).

Evaluation of Phosphate Tridecyl Ethoxylate Triethanolamine Salt as a Corrosion Inhibitor in CO_2-O_2
Environment for Carbon Steel

3

2.4. Surface characterization

To characterize and inspect the reliability of the inhibition phenomenon, the samples of AISI 1018 carbon steel, submitted to different conditions of temperature and PE concentration were investigated in a high-resolution scanning electron microscope (FEG-SEM, FEI-Quanta 450) operating at 20 kV.

2.5. UV/VIS measurement

The UV–vis absorption spectra of the 3.5 *wt*% NaCl solution containing 25 ppm of the inhibitor (PE) with continuous bubbling mixed CO_2-O_2 gas (low dissolved oxygen, 500 ppb) before and after the immersion of the mild steel specimen for 1h at room temperature were measured using a UV-Vis spectrophotometer (Shimadzu model UV-2600 coupled to an ISR 2600 Plus). The UV-Vis spectra of the inhibitor solution are shown as absorbance calculated from reflectance through the Kubelka–Munk transformation.

3. Results

3.1. Electrochemical measurements

3.1.1. Electrochemical impedance spectroscopy (EIS)

The EIS results of carbon steel for conditions with and without corrosion inhibitor at different temperatures are displayed in Figure 2. At 25 °C the blank Nyquist diagram showed three loops, one depressed semicircle associated with the relaxation of the double layer and a charge transfer resistance, followed by an inductive loop and another capacitive

semicircle at a low-frequency range. The inductive loop at a medium frequency can be attributed to the adsorption of intermediate species, $[FeOH]_{ads}$[26,27]. In other temperatures, three loops could also be observed: the capacitive loop at a higher frequency range, which is related to the relaxation of the double layer, and a charge transfer resistance followed by two other faradaic loops.

Keddam et al.[28], Barcia and Mattos[29] investigated the role of chloride and sulfate anions in iron dissolution and concluded that the inductive loop was always associated with the relaxation of $FeOH_{ads}$, independent of the anions. The capacitive loop seen at lower frequencies is related to the relaxation of another species of iron adsorbed on the electrode surface, which has an anion in its structure.

To explain the two faradaic loops, the inductive and the capacitive loop at lower frequencies at 25 °C, Keddam et al.[28] considered a new species adsorbed on the electrode surface and a more complex mechanism. From these reactions, it was possible to write a mechanism with two adsorbed species:
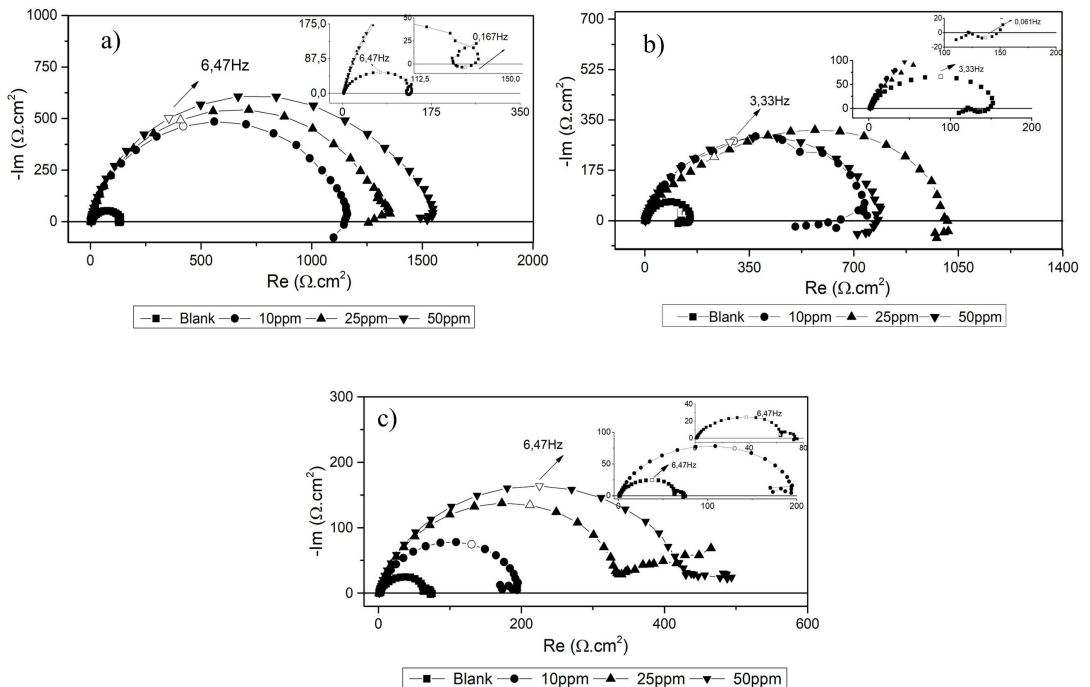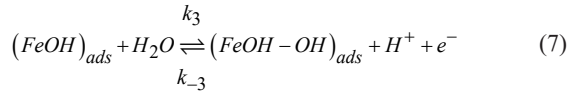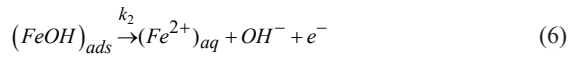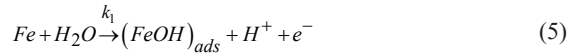
$$Fe + H_2O \xrightarrow{k_1} \left(FeOH\right)_{ads} + H^+ + e^- \qquad (5)$$

$$\left(FeOH\right)_{ads} \xrightarrow{k_2} \left(Fe^{2+}\right)_{aq} + OH^- + e^- \qquad (6)$$

$$\left(FeOH\right)_{ads} + H_2O \underset{k_{-3}}{\overset{k_3}{\rightleftharpoons}} \left(FeOH - OH\right)_{ads} + H^+ + e^- \qquad (7)$$
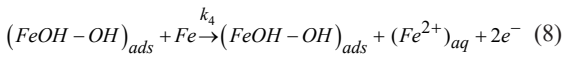

Figure 2. Nyquist plots for AISI 1018 in CO2-O2 3.5wt.% NaCl without and with various concentrations of inhibitor at a) 25 b) 40 and c) 60 °C.

$$\left(FeOH - OH\right)_{ads} + Fe \xrightarrow{k_4} \left(FeOH - OH\right)_{ads} + \left(Fe^{2+}\right)_{aq} + 2e^- \quad (8)$$

The reaction (Equation 8) was presented by Keddam et al.[28] as a self-catalytic reaction[25], i.e., no consumption of $\left(FeOH - OH\right)_{ads}$ happened. In the reaction (Equation 7), Barcia and Mattos[29] proposed that k_3 would be catalyzed by the electrolyte anions, such as chloride or sulfate, depending on the pH range. This kinetic condition has already been discussed, considering that the reactions (Equation 5) and (Equation 6) are only related to H_2O and that neither chloride, sulfate, nor bicarbonate was able to influence the process associated with $(FeOH)_{ads}$[25].

The CO_2 partial pressure effect was studied by Almeida et al.[30] which showed the existence of three loops in the impedance diagrams for different of CO_2 at pH 4. A capacitive loop at higher frequencies, related to the relaxation of the double layer, is followed by two faradaic processes: an inductive loop and a capacitive loop at lower frequencies. The presence of the inductive loop in all experimental conditions was associated with the relaxation of $FeOH_{ads}$ and no direct participation of CO_2 in the electrochemical process was detected.

These works show that neither anion such as chloride or sulfate, nor CO_2 can replace the water on the electrode surface. This suggests that the inductive loop observed herein is related to the relaxation of $FeOH_{ads}$.

The addition of PE seems to inhibit the faradaic processes with the disappearance of the inductive and capacitive loops at lower frequencies and a significant increase in the diameter of the first capacitive loop, with a consequent increase of the charge transfer resistance for all temperatures, indicating its protective ability on CO_2-O_2 environments. From EIS diagrams, the increase in inhibitor concentration provides a marked reduction in the corrosion process. Adding PE to the solution probably changes the time constants of the anodic reactions, mainly k_3 and k_4. Additionally, there is a critical micellar concentration (CMC) concentration above which the inhibition effect will not be enhanced[31,32].

As shown in Table 1, the R_{ct} values after adding PE increase for all temperatures studied. In the testing medium without PE, the values of Rp at 25 oC, 40 oC, and 60 oC are 147.9 Ω cm2, 144.3 Ω cm2, and 72.7 Ω cm2, respectively. With the addition of 25 ppm PE, the Rct values reach 1205.8 Ω cm2, 1130.4 Ω cm2, and 336.7 Ω cm², respectively.

The Bode plots (Figure 3) showed a significant increase in the impedance modulus and phase angle values with PE addition. An increase in the phase angle values of inhibited Bode curves is attributed to the adsorption PE molecules at the metallic surface[33] Hence, the application of phosphate ester as a corrosion inhibitor increases the corrosion resistance of AISI 1018 by adsorbing a protective layer on the steel surface.

3.1.2. Potenciodynamic polarization

The polarization behavior in CO_2-O_2 environment was experimentally investigated on AISI 1018 carbon steel at 25, 40, and 60 ºC, in different PE concentrations. In the blank solution, the anodic polarization process seems to be controlled by a charge transfer reaction since a linear stretch could be observed beyond a decade of current density mainly at 40 and 60 ºC and the cathodic polarization curves show a diffusion-limited cathodic current plateau as shown in Figure 4 probably due to the O_2 reduction.

It can be observed that the curves with inhibitor displace the anodic and cathodic curves to minor current densities relative to the blank, suggesting that the phosphate ester molecules inhibit both anodic and cathodic sites, preventing corrosion attacks. The displacement is more pronounced on the anodic branch. The E_{corr} displaces to more positive potentials with inhibitor addition, showing that PE has an actuation mechanism mixed-type but under anodic control[34,35].

From the curves, it is seen that in the absence and presence of PE, the increase on temperature did not change the carbon steel dissolution in CO_2-saturated 3.5*wt.*% NaCl with DO 500 ppb. For every condition studied, the anodic polarization curves of the inhibited systems show two regions could be identified (Figure 4). The first is Tafel's linear region, then the current increased rapidly and a significant rise in the rate of metal dissolution can be observed. At this point, it is called the desorption potential, E_{des}. Thus, the inhibitor molecules would be considerably desorbed from the electrode surface, and the curves demonstrate that Edes seems to decrease with increasing temperature, suggesting that desorption of the phosphate ester molecules from mild steel surface is favored at higher temperatures at 60 ºC[34,36-38]. Therefore, the phosphate ester exhibits a high corrosion inhibition, thermal stability, and a wide application range in pipelines with varying operational conditions.

3.2. Adsorption isotherm

Adsorption is the main process by which organic inhibitors cover the steel surface and inhibit steel corrosion. The degree of surface coverage, θ, for the concentration range studied was calculated using inhibition efficiency, η, Equation 9[31]:

$$\theta = \eta / 100 \qquad (9)$$

The Langmuir adsorption isotherm showed the best fit among all other available isotherms, such as Freundlich,

Table 1. Electrochemical parameters extracted from impedance data for the C1018 samples exposed to 3.5 wt%NaCl solution saturated with CO_2-O_2 without and with various concentrations of inhibitor.

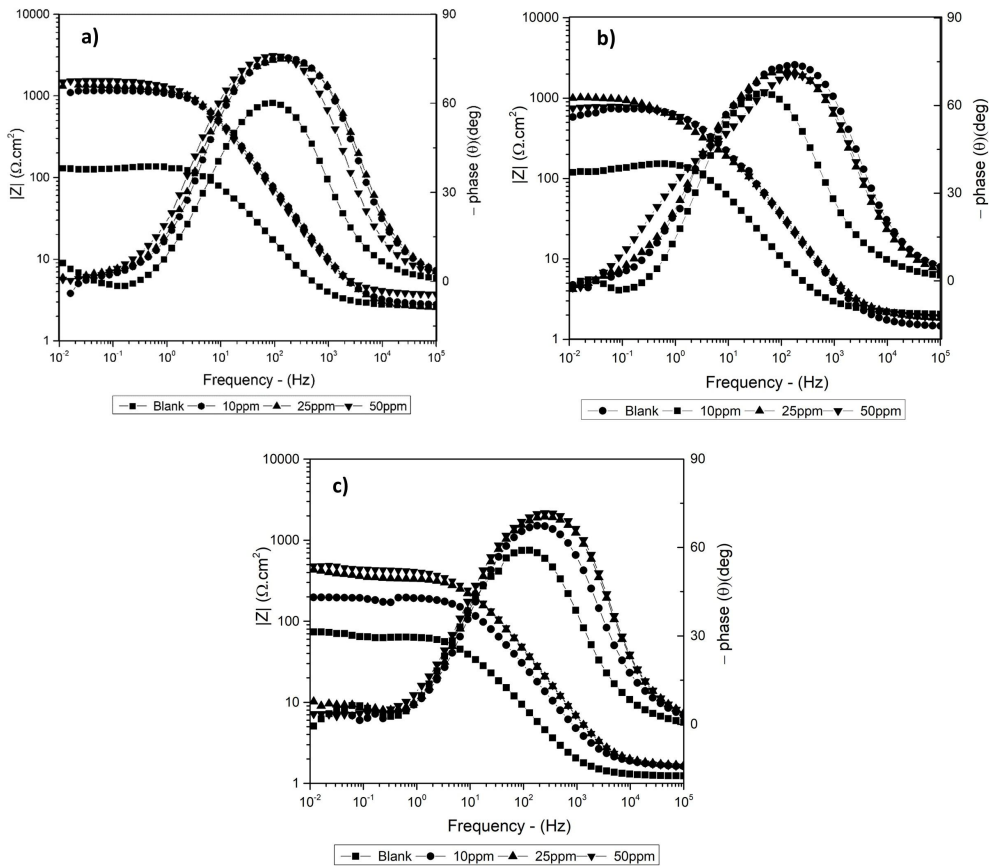| Conc. (ppm)	R_{ct} (Ω.cm²) T 25ºC	R_{ct} (Ω.cm²) T 40ºC	R_{ct} (Ω.cm²) T 60ºC	Ƞ(%) T25ºC	Ƞ(%) T40ºC	Ƞ(%) T 60ºC
Blank	147.9 ± 36.5	144.3 ± 31.8	72.7 ±19.6	-		-
10	1224.9 ± 126.7	787.3 ± 64.4	247.4 ± 31.2	87.9% ± 1.1	81.7% ± 1.6	70.6% ± 13.8
25	1205.8 ± 121.2	1130.4 ± 81.5	336.7 ± 8.31	87.7% ± 1.2	87.2% ± 0.9	78.4% ± 0.5
50	1590.2 ± 55.7	621.9 ± 120.5	436.4 ± 11.5	90.7% ± 0.3	76.8% ± 2.0	83.4% ± 0.4

Figure 3. Bode plots for AISI 1018 in CO2-O2 3.5wt.% NaCl without and with various concentrations of inhibitor at a) 25 °C. b) 40 °C. and c) 60 °C.
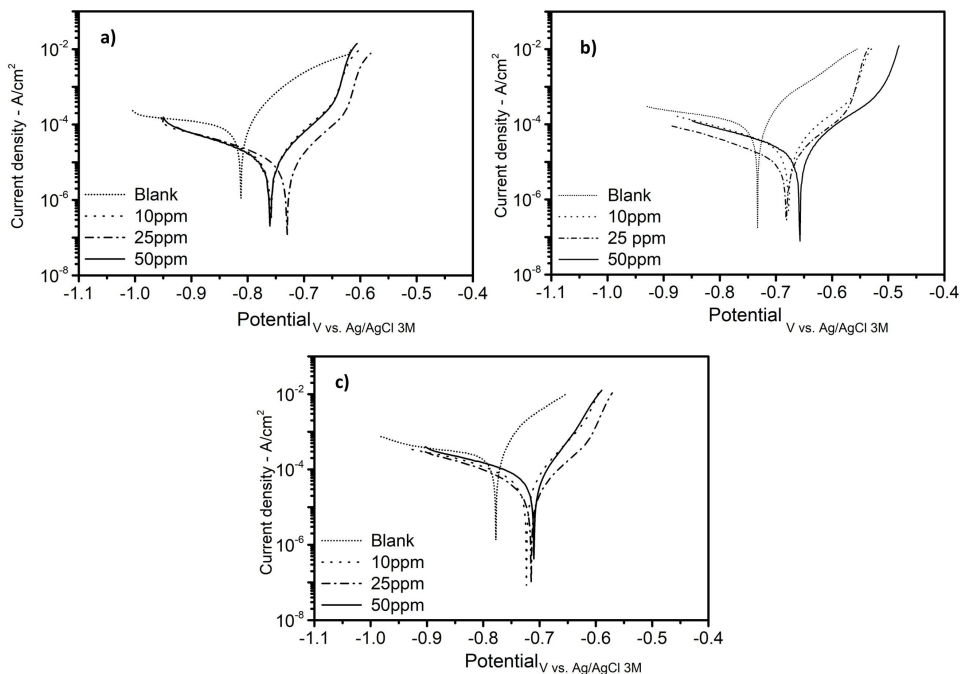

Figure 4. Linear polarization curves for AISI 1018 in CO2-O2 3.5wt.% NaCl without and with various concentrations of inhibitor at a) 25 °C. b) 40 °C. and c) 60 °C.

Frumkin, Temkin, and Flory-Huggins. Langmuir adsorption isotherm for phosphate ester inhibitor could be better explained using the following equation[25]:

$$C / \theta = C + 1 / K_{ads} \qquad (10)$$

Where K_{ads} is the equilibrium constant for the adsorption process, θ is the degree of surface coverage and C is the concentration of the inhibitor. A plot of C/θ *versus* C was drawn to get a straight line (Figure 5). As the mass molar of the PE is unknown, the value of ΔG_{ads} could not be calculated.

3.3. Kinetic parameters study

The essays performed at varying temperatures showed that the corrosion rate (CR) increases both in the absence and the presence of PE inhibitors with increasing temperature (Table 2), and this increase in temperature induces changes in the action of inhibitors. This table shows that the inhibitory efficiency decreases with the increase in temperature. These results suggest that the PE adsorption is physical, with changes in adsorption equilibrium with the temperature. This can alter the strength of the bond between the inhibitor and the metal, causing changes in the equilibrium position. Due to the altered equilibrium at higher temperatures, inhibitors previously adsorbed onto the metal surface might start desorb (detach) from the surface. This is because the increased thermal energy at higher temperatures can break the bonds between the inhibitor molecules and the metal surface, allowing the inhibitors to go back into the solution[39]

The apparent activation energy (E_a) for carbon steel corrosion in the absence and presence of PE was determined by Equation 11[25] (see below), and data in Table 2, resulting in the plot of ln *CR vs.* 1/T (Figure 6).
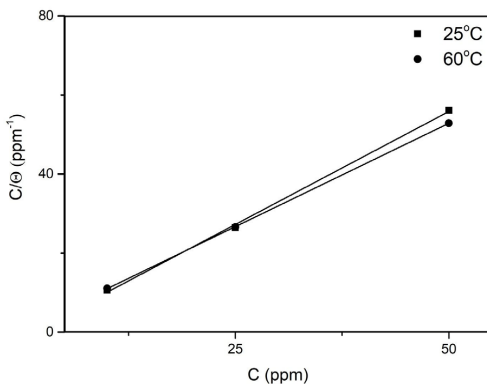
$$\ln CR = lnA - E_a / RT \qquad (11)$$

The apparent activation energy (E_a) for carbon steel corrosion in the absence of PE was 13.6 kJ/mol, whereas in the presence of 25 ppm of PE, it was 56.3 kJ/mol. The apparent activation energy (Ea) in the presence of PE is higher than the blank, suggesting that the adsorption of inhibitor molecules on the metal surface could be physical and indicating a higher energy barrier to corrosion reaction in the presence of PE. Generally, a higher energy barrier reflects the more difficult corrosion reaction[40].

A possible adsorption mechanism is proposed where the oxygen and water molecules approach and quickly adsorb onto the steel surface due to their relatively small size compared to the organic molecules[41]. Moreover, from quantum simulation in previous work, after the addition of PE, the atoms of the phosphate group and the nitrogen atom act as nucleophiles and can directly attach to the steel surface by physisorption and replace the H_2O and O_2 molecules[42].

3.4 Surface Analysis

SEM was used to investigate the role of phosphate ester inhibitors' adsorption on the surface morphology of working electrodes. Figures 7 and 8 show SEM micrographs of the corroded surfaces of steel immersed for 48 h in a CO_2-O_2 3.5 *wt*% NaCl solution at 25 and 60 °C. The corrosion product of samples was removed using Clark solution.

The SEM images for AISI 1018 uninhibited (Figures 7a and 8a) show a general corrosion and delaminated area, indicating a strong attack in both temperatures. Furthermore, the surface exhibits a roughness and irregular profile. The sample morphologies in the solution without PE are consistent with the weight loss measurement results where the corrosion rate
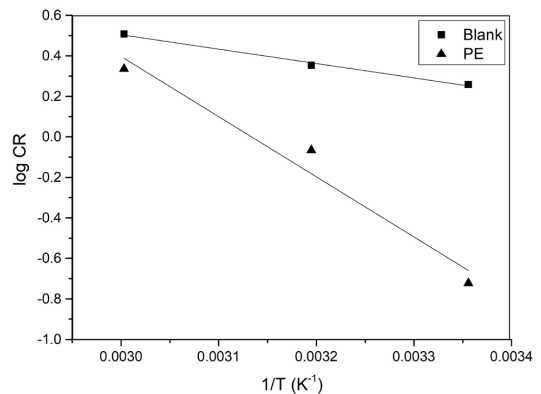

Figure 5. Langmuir isotherm for the adsorption of phosphate ester in CO2-O2 3.5wt.% NaCl at differentTemperatures.

Figure 6. Arrhenius plot for phosphate ester in CO2-O2 3.5wt.% NaCl at 25ppm.

Table 2. Corrosion rates of C1018 samples in 3.5 wt%NaCl solution saturated with CO_2-O_2 and with PE corrosion inhibitor for 24h of immersion time.

Conc. (ppm)	CR mmy 25ºC	CR mmy 40ºC	CR mmy 60ºC	η(%) 25ºC	η(%) 40oC	η(%) 60ºC
Blank	1.81	2.25	3.22			
10	-	-	-	-	-	-
25	0.17	0.92	1.92	90.6% ± 1.0	59.1% ± 2.0	40.4%± 5.1%
50	-	-	-	-	-	-

Evaluation of Phosphate Tridecyl Ethoxylate Triethanolamine Salt as a Corrosion Inhibitor in CO_2-O_2
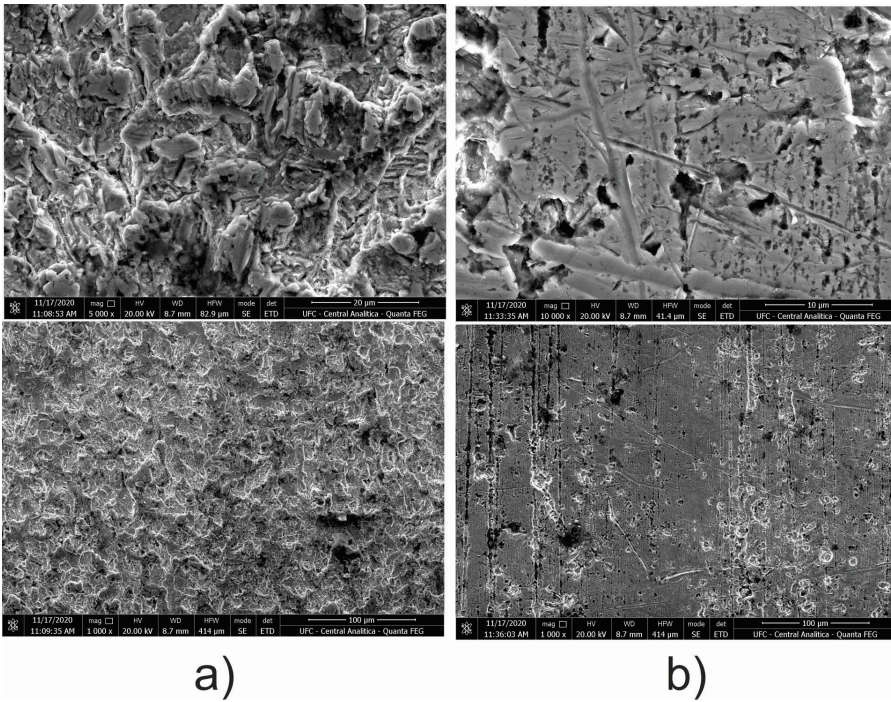Environment for Carbon Steel

7

Figure 7. SEM images of the mild steel surface exposed to 3.5 wt%NaCl solution saturated with CO2-O2 a)Blank at 25 °C, b) with addition of 25ppm PE at 25 °C.
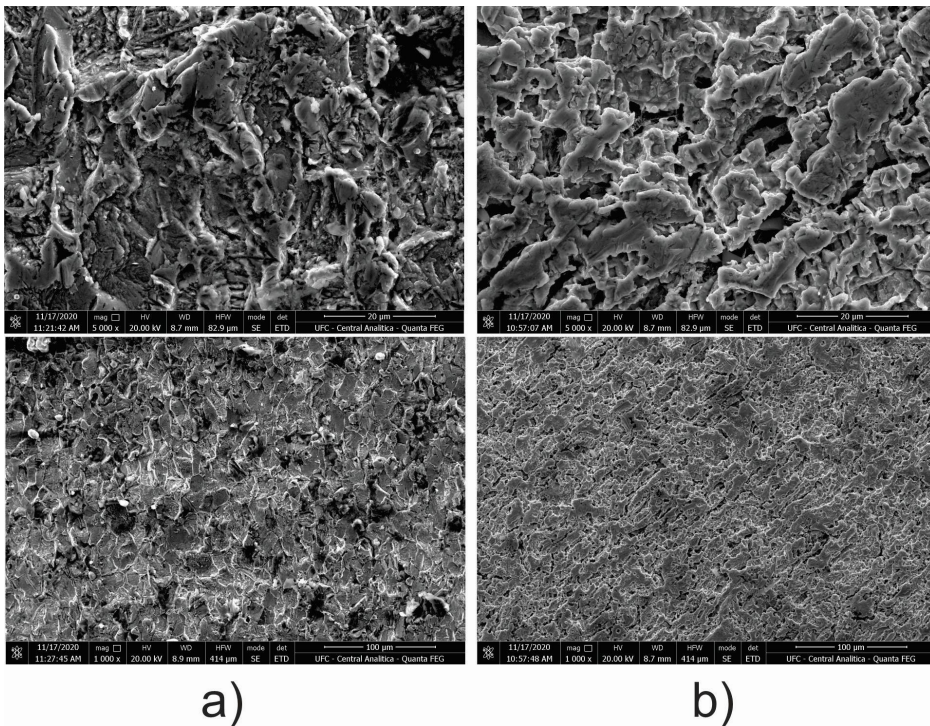

Figure 8. SEM images of the mild steel surface exposed to 3.5 wt%NaCl solution saturated with CO2-O2 a)Blank at 60 °C, b) with addition of 10ppm PE at 60 °C.

for 25 °C and 60 °C are as high as 1.81mmy and 3.22 mmy, respectively. According to Figures 7b and 8b, the addition of phosphate ester into the corrosive media resulted in a surface with some pits, but some scratches from the grinding process exist, showing the suppression of the corrosion process. Hence, PE demonstrates a good inhibition performance
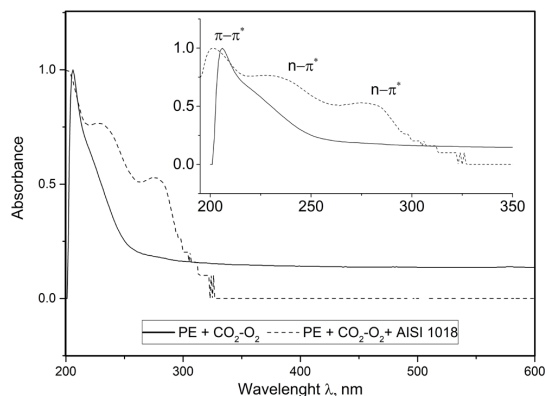
Figure 9. UV–vis spectrum of PE in NaCl 3.5 wt.% containing 25 ppm of the inhibitor (PE) with continuous bubbling mixed CO2-O2 gaslow dissolved oxygen, 500 ppb) before and after the immersion of the mild steel specimen for 1h.

in CO_2-O_2 environments in different conditions of NaCl concentration and temperature. These results corroborate the electrochemical results discussed above.

3.5. UV-VIS

UV–Vis spectroscopy was performed in the bulk solution to indirectly assess the possibility of forming iron/CI complex formation. In metal complexes, the ligands can donate electrons to the metal ion, causing shifts in the energy levels of the d orbitals. This results in the absorption of light at specific wavelengths, giving rise to intense absorption peaks in the UV-visible. The spectrum of PE solution in 3.5*wt*% NaCl before and after 1h of immersion of the 1018 steel sample is shown in Figure 9.

Figure 9 shows the absorbance of phosphate ester PE + CO_2-O_2 and PE + CO_2-O_2 + AISI 1018 in the range of 195-700 nm. PE+ CO_2-O_2 displays one absorption band at 206 nm attributed to π–$\pi*$ vibration of P = O of the phosphate group, while the spectrum containing the mild steel (PE + CO_2-O_2 + AISI 1018) displays three absorption bands at 201, 232, and 278 nm that be assigned as π–$\pi*$ and n –$\pi*$ transition. The new peaks indicate the formation of a complex between the metal surface and the PE molecules[43].

4. Conclusion

The phosphate tridecyl ethoxylate triethanolamine salt (PE) was studied as a corrosion inhibitor for CO_2-O_2 containing in 3.5 *wt*.% NaCl solution at 25 °C, 40 °C and 60 °C. The conclusions are as follows:

1.   PE has a great inhibition efficiency, reaching 90.7% at 25 ppm of concentration at 25 °C, which agrees with electrochemical and weight loss results. It has a wide application range in pipelines with varying operational conditions.

2.   Polarization curves showed a decrease in current density in both anodic and cathodic branches with increased PE concentration. Furthermore, this indicates that the PE acted as a mixed-type inhibitor but under anodic control.

3.   The activation energy increased with the addition of the PE inhibitor. The PE molecules were then

physically adsorbed on the steel surface and obeyed the Langmuir isotherm.

4.   The morphology SEM images confirm that adding PE reduced the corrosion process on carbon steel, and the surface was much less rough than the blank.

5. Acknowledgements

6. References

1.   Gao K, Yu F, Pang X, Zhang G, Qiao L, Chu W, et al. Mechanical properties of CO2 corrosion product scales and their relationship to corrosion rates. Corros Sci. 2008;50(10):2796-803. http://doi.org/10.1016/j.corsci.2008.07.016.

2.   Farelas F, Galicia M, Brown B, Nesic S, Castaneda H. Evolution of dissolution processes at the interface of carbon steel corroding in a CO2 environment studied by EIS. Corros Sci. 2010;52(2):509-17. http://doi.org/10.1016/j.corsci.2009.10.007.

3.   Obuka N, Ikwu ONC, Chukwumuanya GRO, et al. Review of corrosion kinetics and thermodynamics of CO2 and H2S corrosion effects and associated prediction/evaluation on oil and gas pipeline system. Int J Sci Technol Res. 2012;1:156-62.

4.   Verma C, Thakur A, Ganjoo R, Sharma S, Assad H, Kumar A, et al. Coordination bonding and corrosion inhibition potential of nitrogen-rich heterocycles: azoles and triazines as specific examples. Coord Chem Rev. 2023;488:215177. http://doi.org/10.1016/j.ccr.2023.215177.

5.   Li YZ, Xu N, Guo XP, Zhang GA. Inhibition effect of imidazoline inhibitor on the crevice corrosion of N80 carbon steel in the CO2-saturated NaCl solution containing acetic acid. Corros Sci. 2017;126:127-41. http://doi.org/10.1016/j.corsci.2017.06.021.

6.   Zhang H, Gao K, Yan L, Pang X. Inhibition of the corrosion of X70 and Q235 steel in CO2-saturated brine by imidazoline-based inhibitor. J Electroanal Chem (Lausanne). 2017;791:83-94. http://doi.org/10.1016/j.jelechem.2017.02.046.

7.   Zhao J, Gu F, Wang D, Yu M. Effects of thioureido imidazoline on the passivation and pitting corrosion of N80 steel in CO2-saturated NaCl-NaNO2 solution. Int J Electrochem Sci. 2018;13(3):2676-87. http://doi.org/10.20964/2018.03.27.

8.   Zhang J, Gong XL, Yu HH, Du M. The inhibition mechanism of imidazoline phosphate inhibitor for Q235 steel in hydrochloric acid medium. Corros Sci. 2011;53(10):3324-30. http://doi.org/10.1016/j.corsci.2011.06.008.

9.   Jiang X, Zheng Y, Ke W. Corrosion inhibitor performances for carbon dioxide corrosion of N80 steel under static and flowing conditions. Corrosion. 2005;61(4):326-34. http://doi.org/10.5006/1.3279884.

10.   Talkhan AG, Benamor A, Nasser MS, Qiblawey H, El-Tayeb SA, El-Marsafy SM. Corrosion study of carbon steel in CO2 loaded solution of N-methyldiethanolamine and l-arginine mixtures. J Electroanal Chem (Lausanne). 2019;837:10-21. http://doi.org/10.1016/j.jelechem.2019.02.008.

11.   Cen H, Cao J, Chen Z, Guo X. 2-Mercaptobenzothiazole as a corrosion inhibitor for carbon steel in supercritical CO2-H2O condition. Appl Surf Sci. 2019;476:422-34. http://doi.org/10.1016/j.apsusc.2019.01.113.

12.   Cabello G, Funkhouser GP, Cassidy J, Kiser CE, Lane J, Cuesta A. CO and trans-cinnamaldehyde as corrosion inhibitors of I825, L80-13Cr and N80 alloys in concentrated HCl solutions at high pressure and temperature. Electrochim Acta. 2013;97:1-9. http://doi.org/10.1016/j.electacta.2013.03.011.

13. Souza AV, da Rocha JC, Ponciano Gomes JAC, Palermo LCM, Mansur CRE. Development and application of a passion fruit seed oil microemulsion as corrosion inhibitor of P110 carbon steel in CO2-saturated brine. Colloids Surf A Physicochem Eng Asp. 2020;599:124934. http://doi.org/10.1016/j.colsurfa.2020.124934.

14. Yu B, Li DY, Grondin A. Effects of the dissolved oxygen and slurry velocity on erosion–corrosion of carbon steel in aqueous slurries with carbon dioxide and silica sand. Wear. 2013;302(1):1609-14. http://doi.org/10.1016/j.wear.2013.01.044.

15. Martin RL. Corrosion consequences of oxygen entry into oilfield brines. Houston: NACE International; 2002.

16. Hua Y, Barker R, Neville A. The effect of O2 content on the corrosion behaviour of X65 and 5Cr in water-containing supercritical CO2 environments. Appl Surf Sci. 2015;356:499-511. http://doi.org/10.1016/j.apsusc.2015.08.116.

17. Gulbrandsen E, Miland H, Kvarekval J. Effect of oxygen contamination on inhibition studies in carbon dioxide corrosion. Corrosion. 2005;61(11):1086-97. http://doi.org/10.5006/1.3280625.

18. Wang B, Xu L-N, Li D-Y, Lu M-X. Corrosion inhibition mechanism of carbon steel in O2/CO2 coexisting environment. J Mater Eng. 2017;45:38-45. http://doi.org/10.11868/j.issn.1001-4381.2015.000439.

19. Yepez O, Obeyesekere N, Wylde J. Development of novel phosphate based inhibitors effective for oxygen corrosion. Part II: electrochemical characterization. In: NACE - International Corrosion Conference Series 2015; 2015; The Woodland, TX. Proceedings. Houston: NACE International; 2015. p. 1-14.

20. Yepez O, Obeyesekere N, Wylde J. Development of phosphate based inhibitors effective for oxygen corrosion: a study of localized corrosion inhibition mechanism. In: Corrosion/2016; 2016; Houston. Proceedings. Houston: NACE International; 2016. p. 1-15.

21. Hu J, Xiong Q, Chen L, Zhang C, Zheng Z, Geng S, et al. Corrosion inhibitor in CO2-O2-containing environment: inhibition effect and mechanisms of Bis(2-eylhexyl) phosphate for the corrosion of carbon steel. Corros Sci. 2021;179:109173. http://doi.org/10.1016/j.corsci.2020.109173.

22. Merwin A, Chidambaram D. Alternate anodes for the electrolytic reduction of UO2. Metall Mater Trans, A Phys Metall Mater Sci. 2015;46(1):536-44. http://doi.org/10.1007/s11661-014-2633-2.

23. Sanni O, Popoola API, Fayomi OSI. Temperature effect, activation energies and adsorption studies of waste material as stainless steel corrosion inhibitor in sulphuric acid 0.5 M. J Bio Tribocorros. 2019;5(4):88. http://doi.org/10.1007/s40735-019-0280-2.

24. ASTM International. ASTM G1 (2017) Standard Practice for Preparing, Cleaning, and Evaluating Corrosion Test Specimens. West Conshohocken: ASTM International; 2017.

25. da Cunha JN, Evangelista BDV, Xavier AV, da Silva TU, de Oliveira SM, de Araújo JR, et al. Study of furfural derivatives as a possible green corrosion inhibitor for mild steel in CO2-saturated formation water. Corros Sci. 2023;212:110907. http://doi.org/10.1016/j.corsci.2022.110907.

26. Cen H, Chen Z, Guo XN. S co-doped carbon dots as effective corrosion inhibitor for carbon steel in CO2-saturated 3.5% NaCl solution. J Taiwan Inst Chem Eng. 2019;99:224-38. http://doi.org/10.1016/j.jtice.2019.02.036.

27. Okafor PC, Liu X, Zheng YG. Corrosion inhibition of mild steel by ethylamino imidazoline derivative in CO2-saturated solution. Corros Sci. 2009;51(4):761-8. http://doi.org/10.1016/j.corsci.2009.01.017.

28. Keddam M, Mattos OR, Takenouti H. Reaction model for iron dissolution studied by electrode impedance. J Electrochem Soc. 1981;128(2):266-74. http://doi.org/10.1149/1.2127402.

29. Barcia OE, Mattos OR. The role of chloride and sulphate anions in the iron dissolution mechanism studied by impedance

30. measurements. Electrochim Acta. 1990;35(6):1003-9. http://doi.org/10.1016/0013-4686(90)90035-X.

30. Almeida TC, Bandeira MCE, Moreira RM, et al. New insights on the role of CO2 in the mechanism of carbon steel corrosion. Corros Sci. 2017;120:239-50. http://doi.org/10.1016/j.corsci.2017.02.016.

31. Pakiet M, Kowalczyk IH, Leiva Garcia R, Akid R, Brycki BE. Influence of different counterions on gemini surfactants with polyamine platform as corrosion inhibitors for stainless steel AISI 304 in 3 M HCl. J Mol Liq. 2018;268:824-31. http://doi.org/10.1016/j.molliq.2018.07.120.

32. Chauhan DS, Quraishi MA, Jafar Mazumder MA, Ali SA, Aljeaban NA, Alharbi BG. Design and synthesis of a novel corrosion inhibitor embedded with quaternary ammonium, amide and amine motifs for protection of carbon steel in 1 M HCl. J Mol Liq. 2020;317:113917. http://doi.org/10.1016/j.molliq.2020.113917.

33. Verma C, Quraishi MA. Recent progresses in Schiff bases as aqueous phase corrosion inhibitors: design and applications. Coord Chem Rev. 2021;446:214105. http://doi.org/10.1016/j.ccr.2021.214105.

34. Cen H, Cao J, Chen Z. Functionalized carbon nanotubes as a novel inhibitor to enhance the anticorrosion performance of carbon steel in CO2-saturated NaCl solution. Corros Sci. 2020;177:109011. http://doi.org/10.1016/j.corsci.2020.109011.

35. Fernandes CM, Alvarez LX, dos Santos NE, Maldonado Barrios AC, Ponzio EA. Green synthesis of 1-benzyl-4-phenyl-1H-1,2,3-triazole, its application as corrosion inhibitor for mild steel in acidic medium and new approach of classical electrochemical analyses. Corros Sci. 2019;149:185-94. http://doi.org/10.1016/j.corsci.2019.01.019.

36. Zhang X, Wang F, He Y, Du Y. Study of the inhibition mechanism of imidazoline amide on CO2 corrosion of Armco iron. Corros Sci. 2001;43(8):1417-31. http://doi.org/10.1016/S0010-938X(00)00160-8.

37. Desimone MP, Gordillo G, Simison SN. The effect of temperature and concentration on the corrosion inhibition mechanism of an amphiphilic amido-amine in CO2 saturated solution. Corros Sci. 2011;53(12):4033-43. http://doi.org/10.1016/j.corsci.2011.08.009.

38. Yıldız R, Döner A, Doğan T, Dehri İ. Experimental studies of 2-pyridinecarbonitrile as corrosion inhibitor for mild steel in hydrochloric acid solution. Corros Sci. 2014;82:125-32. http://doi.org/10.1016/j.corsci.2014.01.008.

39. El-Azabawy OE, Higazy SA, Al-Sabagh AM, Abdel-Rahman AAH, Nasser NM, Khamis EA. Studying the temperature influence on carbon steel in sour petroleum media using facilely-designed Schiff base polymers as corrosion inhibitors. J Mol Struct. 2023;1275:134518. http://doi.org/10.1016/j.molstruc.2022.134518.

40. Akpan ED, Kumar Singh A, Lgaz H, Quadri TW, Kumar Shukla S, Mangla B, et al. Coordination compounds as corrosion inhibitors of metals: a review. Coord Chem Rev. 2024;499:215503. http://doi.org/10.1016/j.ccr.2023.215503.

41. Zhang QH, Hou BS, Li YY, Zhu GY, Lei Y, Wang X, et al. Dextran derivatives as highly efficient green corrosion inhibitors for carbon steel in CO2-saturated oilfield produced water: experimental and theoretical approaches. Chem Eng J. 2021;424:130519. http://doi.org/10.1016/j.cej.2021.130519.

42. Vasques RB, Levy MM, Rodrigues MS, de Queiroz Almeida Neto FW, da Silva LP, Vaz GL, et al. A theoretical and experimental study of phosphate ester inhibitors for AISI 1018 in carbon dioxide-saturated 3.5 wt% NaCl solution. Mater Corros. 2021;72(8):1417-32. http://doi.org/10.1002/maco.202112365.

43. Haldhar R, Prasad D, Saxena A, Kumar R. Experimental and theoretical studies of Ficus religiosa as green corrosion inhibitor for mild steel in 0.5 M H2SO4 solution. Sustain Chem Pharm. 2018;9:95-105. http://doi.org/10.1016/j.scp.2018.07.002.